PERGAMON

International Journal of Heat and Mass Transfer 43 (2000) 3795–3810

International Journal of HEAT and MASS TRANSFER

www.elsevier.com/locate/ijhmt

Design and control of interfacial temperature gradients in solidification

S.W. Hale*, M. Keyhani, J.I. Frankel

Mechanical & Aerospace Engineering and Engineering Science Department, University of Tennessee, Knoxville, TN 37996-2210, USA

Received 23 March 1999; received in revised form 16 December 1999

Abstract

In a unidirectional solidification design problem, the solidification velocity and the liquid-side interfacial temperature gradient are of principle interest due to their effect on the morphology of the cast structure. The design challenge is prediction of the temporal conditions at the boundaries, such that the solidification velocity and the liquid-side temperature gradient at the solid–liquid interface follow a predetermined design scenario. The stated problem requires the resolution of two inverse problems: one, in an expanding solid domain and the second, in a shrinking liquid domain. An innovative solution technique is proposed and demonstrated for design of the liquid-side temperature gradient during unidirectional solidification. During the early transient, the control of the interfacial temperature gradient presents a challenge due to the diffusion time between the boundary and the interface. This challenge is met using a combination of initial condition design and time structuring, which allows independent control of the interfacial temperature gradient for the extent of the solidification process. The solution is developed in the context of a classic weighted-residual method, where the temporal variable is treated in an elliptic fashion.

1. Introduction

To assure the quality and reliability of a casting, the ability to predict and control its morphology is of paramount importance. The main parameters governing the morphology during the casting process are the solidification velocity, V, and the liquid-side interfacial temperature gradient G_l [1–3]. The ability to control the microstructure of a casting possesses the potential to produce a desired morphology, which can have a profound effect on the metallurgical properties of the casting. It is expected [3] that the movement towards directionally solidified and single-crystal castings will continue to grow, since the resulting microstructure provides the materials with improved strength at high temperatures and better thermal fatigue resistance.

The rationale for proposing the inverse solidification design problem, illustrated in Fig. 1, lies in the development of a controlled cast structure. In order to produce such a controlled cast structure, one must possess the ability to exert independent control of the solidification velocity, $V(t)$, and the liquid-side interfacial temperature gradient $G_l(t)$.

The body of literature concerned with inverse analysis of solidification problems is relatively limited. Various methodologies have been proposed to resolve this class of inverse problems, with varying degrees of success [4–12]. The authors are unaware, however, of any studies that directly address the resolution of the solidification design problem in which independent control of the interfacial velocity,

* Corresponding author.

0017-9310/00/$ - see front matter
PII: S0017-9310(00)00011-9

Nomenclature

$a_k(\xi)$	time varying expansion coefficients
$b_k(\xi)$	re-indexed time varying expansion coefficients
$c_{j,\,k}$	expansion coefficients
c_p	specific heat
$d_{j,\,k}$	re-indexed expansion coefficient
$G(t)$	interfacial temperature gradient
G_d	design liquid-side interfacial temperature gradient
G_i	initial temperature gradient
$h(\xi)$	mapped interfacial location
$h(\xi)$	mapped interfacial velocity
h_f	heat of fusion
k	thermal conductivity
$\mathscr{L}$	spatial extent of analysis
$\mathscr{L}$	differential operator
$\mathscr{S}\mathscr{C}\bar{\mathscr{L}}$	mapped differential operator
N	terms in spatial expansion
P	terms in temporal expansion
$q_c''(t)$	cold wall heat flux
$q_h''(t)$	hot wall heat flux
$R(\theta(\eta,\,\xi))$	Residual function
$s(t)$	interfacial location
t	temporal coordinate
t_f	time at which $T_0(t)$ reaches T_f
t_g	time at which $G_l(t)$ reaches G_d
t_{max}	temporal extent of analysis
t_p	penetration time
t_v	time at which $V(t)$ reaches V_d
$T(x,\,t)$	temperature
$T_c(t)$	cold wall temperature history
T_f	fusion temperature
$T_h(t)$	hot wall temperature history
$T_i(x)$	initial temperature distribution
$T_k(\eta)$	Chebyshev polynomial of the first kind
$T_0(t)$	interfacial temperature history
$V(t)$	interfacial velocity
V_d	design interfacial velocity
x	spatial coordinate

Greek symbols

α	thermal diffusivity
$\Gamma(\xi)$	mapped interfacial temperature gradient
δ	dirac delta function
Δ	mapped interfacial location
η	spatial mapping variable
η_{l_0}	modified liquid spatial mapping function
$\theta(\eta,\,\xi)$	mapped temperature
$\theta_c(\xi)$	mapped cold wall temperature history
$\theta_h(\xi)$	mapped hot wall temperature history
$\theta_i(\eta_{l_0})$	mapped initial temperature distribution
$\theta_0(\xi)$	mapped interfacial temperature history
ξ	temporal mapping variable
ρ	density
$\psi(\eta,\,\xi)$	boundary condition series function
$\omega_k(\eta)$	spatial trial function
$\Omega_{j,\,k}(\eta,\,\xi)$	combine spatial-temporal trial function

Subscripts

l	liquid quantity
s	solid quantity

Superscript

N	denotes approximation of quantity

$V(t)$, and liquid-side interfacial temperature gradient, $G_l(t)$, has been demonstrated.

Zabaras, Mukherjee, and Richmond [4], investigated the application of an integral method combined with the sensitivity analysis technique of Beck, Blackwell, and St. Clair, Jr. [13] to resolve an inverse solidification problem. In the resolution of the solid domain, overspecified interfacial conditions of $V(t) = C$ and $G_l(t) = 0$ were utilized. The exact solution for this problem is given in [14]. The interfacial conditions used in the resolution of the liquid domain, however, where unrelated to the solid domain. Specifically, the exact solution of a one-phase supercooled solidification problem, given in [14,15], was used to specify $V(t)$ and $G_l(t)$ for the liquid domain. The results obtained utilizing the proposed methodology agreed well with the analytical solutions. However, the problem investigated did not address the issue of independent control of the solidification velocity, $V(t)$, and the liquid-side interfacial temperature gradient, $G_l(t)$.

Similarly, Zabaras in [6] applied a finite element technique coupled with the future information method of Beck et al. [13] to resolve two types of inverse solidification problems. The first type was identical to that discussed above in that overspecified interface conditions, i.e., $V(t)$ and $G_l(t)$, were utilized to predict the unknown boundary conditions. The second type involved the use of discrete data, i.e., thermocouple temperature measurements, to resolve the unknown boundary conditions and interface information. Of these two, only the first type is of interest to this exposition. The application of the proposed methodology was illustrated utilizing the same analytical solutions described above [14,15]. That is, analytical solutions are used to generate the overspecified interface data,

i.e., $V(t)$ and $G_l(t)$, for solution of the solid and liquid domains as well as to provide a measure of accuracy for the results. Again, though the results matched well, the problem investigated did not address the solidification design problem with independent $V(t)$ and $G_l(t)$ control.

More recently, Yang and Zabaras have investigated the design of solidification processes in the presence of natural convection in the liquid for both pure and binary melts. In [16] the authors apply the Adjoint method to resolve a pure melt solidification design problem for which the goal is the preservation of a flat planer interface moving at a known time varying velocity. The design scenario is constructed utilizing the direct solution of a one-dimensional two-phase Stefan problem, with no convection in the liquid. Since the solution to this type problem naturally gives rise to a flat planer interface, the resulting $V(t)$ and $G_l(t)$, when utilized in an inverse design analysis, will predict the desired boundary conditions. It should be noted that both the interfacial velocity and liquid-side interfacial temperature gradient vary in time and will thus result in a non-uniform microstructure in the final casting. Similarly, in [17] the authors apply the Adjoint method to the resolution of a binary melt solidification design problem in which again the goal is the preservation of a flat planer interface moving at a constant velocity. A combination of direct solidification analysis along with the stability requirement that at any time there is no constitutional undercooling in the liquid defines the design scenario for $V(t)$ and $G_l(t)$. The results given indicate that though a constant solidification velocity is obtained, the liquid-side interfacial temperature gradient varies in time and thus again gives rise to a non-uniform microstructure. Moreover, the resulting liquid-side interfacial temperature gradient cannot be influenced to follow a desired path and is completely dependent on the selected design scenario for the interfacial velocity.

The objective of the current exposition is to present an overall methodology for the resolution of a unidirectional solidification design problem. The methodology consists of a set design or parameter scenarios combined with a stable numerical technique: the Global Time Method (GTM) proposed by Frankel and Keyhani [12]. These scenarios are constructed such that the physics of the problem are taken into account while allowing independent control of solidification velocity, $V(t)$, and liquid-side interfacial temperature gradient, $G_l(t)$.

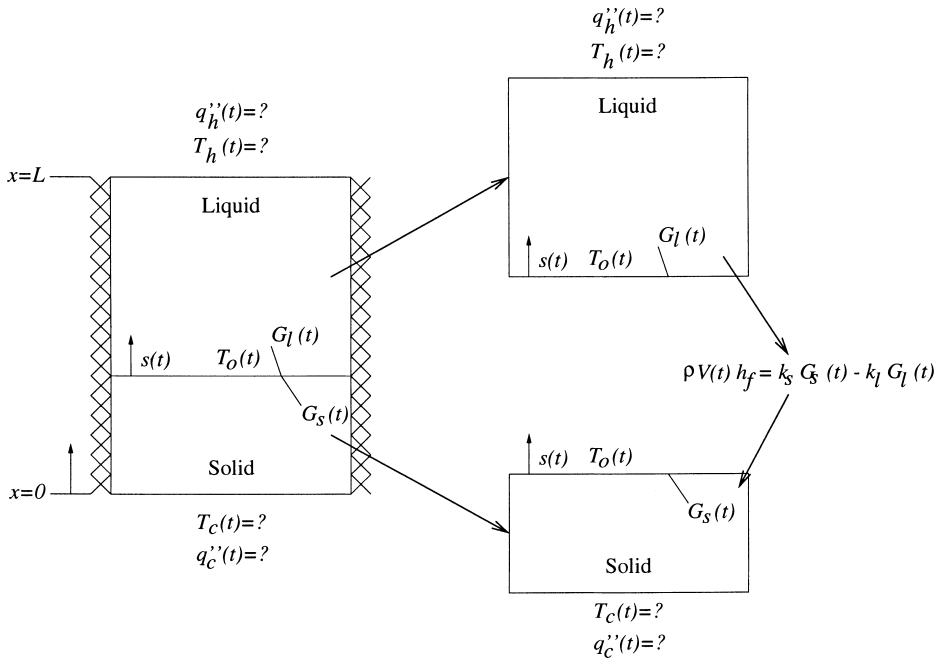

Fig. 1. Schematic of the pure melt solidification design problem illustrating the splitting of the solid and liquid domains.

2. Design scenario

The challenge in the design of a solidification process is the approximation of a set of boundary conditions, either surface temperature or heat flux histories, that when imposed will produce the prescribed solid–liquid interfacial motion and liquid-side temperature gradient. Upon closer examination, it can be seen that this design problem can be broken down into two uncoupled inverse heat conduction problems, each on a deforming domain as shown in Fig. 1. Resolution of the liquid region determines the hot wall temperature history, $T_h(t)$, required to reproduce the specified liquid-side interfacial temperature gradient, $G_l(t)$. Similarly, resolution of the solid region determines the cold wall temperature history, $T_c(t)$, required to affect the desired interfacial motion, $s(t)$.

Though resolution of either the solid or liquid region presents a considerable challenge due to the mildly ill-posed nature of the problem, the liquid region has an additional difficulty associated with the diffusive nature of heat conduction. Consider the initial stages of a unidirectional solidification process. At the instant solidification begins, the temporal evolution of $G_l(t)$ is governed by the velocity of the solid–liquid interface and the initial temperature distribution near the interface. Since the interfacial motion, $s(t)$, is a design parameter and thus must follow a predetermined scenario, it is not a 'free' parameter that can be utilized for $G_l(t)$ control. Therefore, the only means by which control of $G_l(t)$ may be realized is through the control of the superheat distribution near the interface, such that, in conjunction with the prescribed interfacial velocity, $V(t)$, the desired temporal behavior of $G_l(t)$ is obtained. The only 'free' parameter available which can be utilized in controlling the superheat distribution near the interface is $T_h(t)$. However, any changes in $T_h(t)$ initiated at the instant solidification begins will alter the temperature distribution near the interface, and thus $G_l(t)$, only after the required diffusion time has elapsed. Therefore, active control of $G_l(t)$ at time t requires the alteration of $T_h(t)$ at time $t - t_p$, where t_p is the diffusion time required for a thermal front initiated at $x = L$ to penetrate the liquid domain and reach the solid–liquid interface at $x = s(t)$. To accommodate this penetration time, the temporal extent of the analysis domain must be extended such that sufficient lead time is provided for the control signals, i.e., alterations of $T_h(t)$, to reach the interface.

The preceding discussion illustrates that active control of $G_l(t)$ is a complex task and why independent control of $V(t)$ and $G_l(t)$ was thought impossible. This idea of extending the temporal domain of the analysis into an area prior to the start of solidification has not been implemented in any of the previous design studies of this nature. To illustrate its implementation, a typical scenario will be discussed applicable to the current design problem. Consider a melt having an initial temperature distribution $T_i(x)$ at time $t = 0$, with $T_i(0) \geq T_f$ where T_f is the fusion temperature of the material. For the time period $0 \leq t \leq t_p$, the surface temperature at $x = 0$, which corresponds to the interface position for this time period, is maintained at its initial value of $T_i(0)$ as shown in Fig. 2(a). Following this holding period, the surface is cooled from $T_i(0)$ to T_f in the time period $t_p \leq t \leq t_f$. Once the surface temperature has reached T_f, any further cooling would result in the initiation of solidification, and the solid–liquid interface would separate from the bottom surface and its temperature would remain at T_f as shown in Fig. 2(a).

The solidification is specified to commence at $t > t_f$, and proceed with a design velocity of $V(t)$, which is specified to change from zero to a constant value of V_d during the time period $t_f \leq t \leq t_v$ as shown in Fig. 2(b). For this design velocity, $V(t)$, solidification of a region of length L would require a time period of $t_{max} - t_f$. To demonstrate the ability to independently control $G_l(t)$ via active control of $T_h(t)$, a design scenario for $G_l(t)$ must be specified which is uncoupled from $V(t)$. The proposed design scenario for the temporal evolution of $G_l(t)$ is illustrated in Fig. 2(c). During the time period $0 \leq t \leq t_p$, $G_l(t)$ will be at its initial value of G_i, corresponding to the specified initial distribution of $T_i(x)$. Recall that for $t \geq t_p$ the surface at $x = 0$ is being cooled resulting in an immediate change in $G_l(t)$. Therefore, we require $G_l(t)$ to change from its initial value of G_i to its design value of G_d in the time interval $t_p \leq t \leq t_g$.

At this point, the design scenario for inverse analysis of the liquid domain is complete. Namely, in the time domain $0 \leq t \leq t_{max}$, the solid–liquid interface must move with the design velocity, $V(t)$, and at $x = s(t)$ be subject to the overspecified interfacial conditions of temperature, $T_0(t)$, and temperature gradient, $G_l(t)$. Based on this scenario, solidification proceeds with a constant velocity of V_d for $t \geq t_v$, and a constant liquid-side interfacial temperature gradient of G_d for $t \geq t_g$.

3. Mathematical formulation

3.1. Governing equations

Consider the unidirectional solidification of a pure material or eutectic binary alloy. Assuming that the solid and liquid phases have equal densities, i.e., no bulk motion occurs in the liquid domain, the equation describing energy transport in the solid and liquid regions is the standard heat equation.

Solid: $\mathscr{L}_s[T(x,t)] = 0, \quad t > t_f, \quad x \in (0, s(t))$ (1a)

Liquid: $\mathscr{L}_l[T(x,t)] = 0, \quad t > 0, \quad x \in (s(t), L),$ (1b)

where the differential operators, $\mathscr{L}_l$ and $\mathscr{L}_s$, are given by

$$\mathscr{L}_j = k_j \frac{\partial^2}{\partial x^2} - \rho c_{p_j} \frac{\partial}{\partial t}, \quad j = l, s. \tag{1c}$$

The over-specified interfacial conditions are of the form

$$T(s(t), t) = T_{0.}(t), \quad t > 0 \tag{1d}$$

$$\left.\frac{\partial}{\partial x} T(x,t)\right|_{x=s+(t)} = G_l(t), \quad t > 0, \tag{1e}$$

$$\left.\frac{\partial}{\partial x} T(x,t)\right|_{x=s^-(t)} = G_s(t), \quad t > t_f \tag{1f}$$

and the initial condition is given by

$$T(x,0) = T_i(x), \quad x \in [0, L]. \tag{1g}$$

The solid and liquid-side interfacial temperature gradients, $G_s(t)$ and $G_l(t)$, are related via the classical Stefan condition,

$$\rho V(t) h_f = k_s G_s(t) - k_l G_l(t), \quad t > t_f \tag{2}$$

where h_f is the heat of fusion of the material.

As stated earlier, resolution of the liquid domain requires the determination of the hot wall temperature history, which will reproduce the desired liquid-side interfacial temperature gradient. Similarly, the solid domain requires the resolution of the cold wall temperature history, which will reproduce the desired interfacial motion. Mathematically speaking, we seek

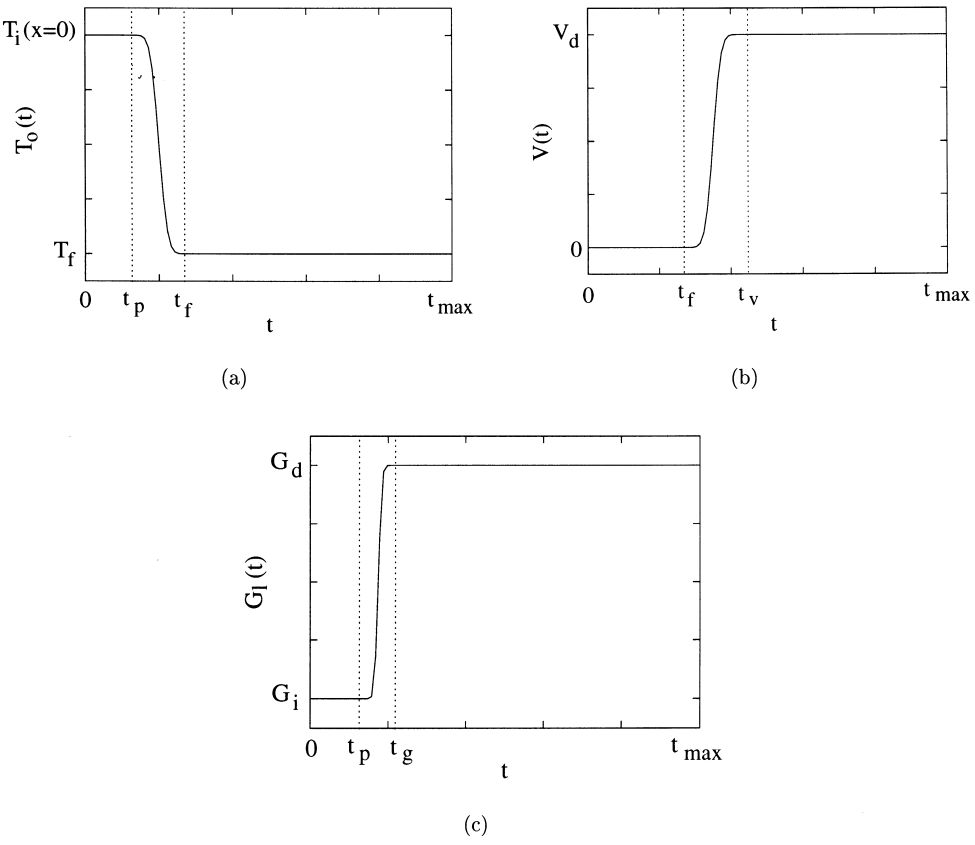

Fig. 2. Illustration of the temporal evolution of the solidification design problem: (a) interface temperature function; (b) interface velocity function; (c) gradient liquid-side interfacial temperature gradient function.

knowledge of

$$T(L, t) = T_h(t) = ?, \quad t > 0. \tag{3a}$$

$$T(0, t) = T_c(t) = ?, \quad t > 0. \tag{3b}$$

3.2. Coordinate mapping

To comply with restrictions imposed by the basis functions utilized in the numerical analysis, the independent coordinates must be mapped onto a fixed domain bounded by ± 1.

3.3. Liquid domain

For the liquid domain, this mapping is accomplished utilizing the following linear coordinate transforms:

$$\eta_l(x, t) = 2\left(\frac{x - L}{L - s(t)}\right) + 1, \quad \eta_l \in [-1, 1], \tag{4a}$$

$$\xi_l(x, t) = 2\left(\frac{t}{t_{max}}\right) - 1, \quad \xi_l \in [-1, 1], \tag{4b}$$

where, again, $s(t)$ is the solid–liquid interface position, L is the spatial extent of the analysis, and t_{max} is the temporal extent of the analysis. Treating these new coordinates as independent variables and using the chain rule, Eq. (1b) can be recast as

$$\bar{\mathscr{L}}_l\left[\theta_l(\eta_l, \xi_l)\right] = 0, \quad (\eta_l, \xi_l) \in (-1, 1), \tag{5a}$$

where the mapped differential operator, $\bar{\mathscr{L}}_l$, is given by

$$\bar{\mathscr{L}}_l = \frac{\partial^2}{\partial \eta_l^2} - \frac{(L - h_l(\xi_l))^2}{2\alpha_l t_{max}}\left(\frac{\eta_l - 1}{L - h_l(\xi_l)}\dot{h}_l(\xi_l)\frac{\partial}{\partial \eta_l} + \frac{\partial}{\partial \xi_l}\right), \tag{5b}$$

$$(\eta_l, \xi_l) \in (-1, 1),$$

with

$$\theta_l(\eta_l, \xi_l) = T\left((\eta_l - 1)\frac{L - h_l(\xi_l)}{2} + L, (\xi_l + 1)\frac{t_{max}}{2}\right),$$

$$h_l(\xi_l) = s\left((\xi_l + 1)\frac{t_{max}}{2}\right)$$

$$\dot{h}_l(\xi_l) = \frac{d}{d\xi_l}h_l(\xi_l), \qquad \alpha_l = \frac{k_l}{\rho c_{pl}}.$$

In a similar manner, the over-specified interfacial conditions can be recast as

$$\theta_l(-1, \xi_l) = \theta_{l_0}(\xi_l), \quad \xi_l \in (-1, 1) \tag{6a}$$

$$\frac{\partial}{\partial \eta_l}\theta_l(\eta_l, \xi_l)\Big|_{\eta_l = -1} = \Gamma_l(\xi_l), \quad \xi_l \in (-1, 1) \tag{6b}$$

where

$$\theta_{l_0}(\xi_l) = T_0\left((\xi_l + 1)\frac{t_{max}}{2}\right),$$

$$\Gamma_l(\xi_l) = \frac{L - h_l(\xi_l)}{2}G_l\left((\xi_l + 1)\frac{t_{max}}{2}\right).$$

The recasting of the initial condition presents a challenge due to the fact that we have chosen to treat η_l and ξ_l as independent variables. To circumvent this, we must define a special value of η_l that has been 'evaluated' at $\xi_l = -1$ to account for the fact that the initial condition is being drawn from a fixed coordinate frame. Let

$$\eta_{l_0} = 2\left(\frac{x}{L}\right) - 1, \quad \eta_{l_0} \in [-1, 1], \tag{7a}$$

such that

$$\eta_{l_0} = (\eta_l - 1)\left(\frac{L - h_l(\xi_l)}{L}\right) + 1. \tag{7b}$$

Evaluating $\theta_l(\eta_l, \xi_l)$ at $\xi_l = -1$, and noting that $\eta_{l_0} = \eta_l$, the initial condition can be recast as

$$\theta_l(\eta_l = \eta_{l_0}, -1) = \theta_i(\eta_{l_0}), \quad \eta_{l_0} \in [-1, 1], \tag{8}$$

where

$$\theta_i(\eta_{l_0}) = T_i\left((\eta_{l_0} + 1)\frac{L}{2}\right).$$

Finally, the unknown hot wall boundary condition can be recast as

$$\theta_l(1, \xi_l) = \theta_h(\xi_l), \quad \xi_l \in (-1, 1), \tag{9}$$

with

$$\theta_h(\xi_l) = T_h\left((\xi_l + 1)\frac{t_{max}}{2}\right).$$

3.4. Solid domain

For the solid domain, a similar set of linear coordinate transformations are utilized. Let

$$\eta_s(x, t) = 2\left(\frac{x}{s(t)}\right) - 1, \quad \eta_s \in [-1, 1], \tag{10a}$$

$$\xi_s(x,t) = 2\left(\frac{t-t_f}{t_{max}-t_f}\right) - 1, \quad \xi_s \in (-1,1). \tag{10b}$$

Again, treating these coordinates as independent variables and applying the chain rule, the governing Eq. (1a), can be recast as

$$\bar{\mathscr{L}}_s\left[\theta_s(\eta_s,\xi_s)\right] = 0, \quad (\eta_s,\xi_s) \in (-1,1) \tag{11a}$$

The mapped differential operator, $\bar{\mathscr{L}}_s$, is given by

$$\bar{\mathscr{L}}_s = \frac{\partial^2}{\partial\eta_s^2} - \frac{h_s^2(\xi_s)}{2\alpha_s(t_{max}-t_f)}\left(-\frac{\eta_s+1}{h_s(\xi_s)}\dot{h}_s(\xi_s)\frac{\partial}{\partial\eta_s} + \frac{\partial}{\partial\xi_s}\right), \quad (\eta_s,\xi_s) \in (-1,1) \tag{11b}$$

where

$$\theta_s(\eta_s,\xi_s) = T\left((\eta_s+1)\frac{h_s(\xi_s)}{2}, (\xi_s+1)\frac{t_{max}-t_f}{2} + t_f\right),$$

$$h_s(\xi_s) = s\left((\xi_s+1)\frac{t_{max}-t_f}{2} + t_f\right),$$

$$\dot{h}_s(\xi_s) = \frac{d}{d\xi_s}h_s(\xi_s), \qquad \alpha_s = \frac{k_s}{\rho c_{p_s}}.$$

Proceeding in a similar manner, the mapped over-specified interfacial conditions are given by

$$\theta_s(1,\xi_s) = \theta_{s_0}(\xi_s), \quad \xi_s \in (-1,1) \tag{12a}$$

$$\frac{\partial}{\partial\eta_s}\theta_s(\eta_s,\eta_s)\xi_s\Big|_{\eta_s=1} = \Gamma_s(\xi_s), \quad \xi_s \in (-1,1), \tag{12b}$$

where

$$\theta_{s_0}(\xi_s) = T_0\left((\xi_s+1)\frac{t_{max}-t_f}{2} + t_f\right),$$

$$\Gamma_s(\xi_s)\frac{h_s(\xi_s)}{2}G_s\left((\xi_s+1)\frac{t_{max}-t_f}{2} + t_f\right).$$

Due to the uncoupling of the solid and liquid domains, an initial condition must be formulated for the solid domain. Recall from the discussion of Fig. 2 that for $t \geq t_f$ we require $T_0(t) = T_f$. Rearranging Eq. (10a)

$$x = (\eta_s+1)\frac{h_s(\xi_s)}{2},$$

evaluating it at $\xi_s = -1$, and noting that $h_s(-1) = 0$, it can clearly be seen that $x = 0$ is mapped onto $-1 \leq \eta_s \leq 1$. Therefore, by forcing Eq. (12a) to be satisfied at $\xi_s = -1$, to provide continuity of temperature at the boundary, we require

$$\theta_s(\eta_s,-1) = \theta_{s_0}(-1) = T_f, \quad \eta_s \in [-1,1]. \tag{13}$$

Lastly, the unknown cold wall boundary condition can be recast as

$$\theta_s(-1,\xi_s) = \theta_c(\xi_s), \quad \xi_s \in (-1,1), \tag{14}$$

where

$$\theta_c(\xi_s) = T_c\left((\xi_s+1)\frac{t_{max}-t_f}{2} + t_f\right)$$

To complete the transformation of the solid domain, the Stefan condition shown in Eq. (2) must also be mapped onto a fixed domain. With regard to the mapping of the temporal variable, two possibilities exist, ξ_s or ξ_l. Since the Stefan condition is only valid during solidification, its temporal domain is limited to $t_f < t \leq t_{max}$, which corresponds to the ξ_s mapping. Therefore, utilizing Eq. (10b) the Stefan condition can be recast as

$$\Gamma_s(\xi_s) = \frac{h_s(\xi_s)}{2k_s}\left(\frac{2}{t_{max}-t_f}\rho h_f\dot{h}_s(\xi_s) + k_l G_l\left((\xi_s+1)\frac{t_{max}-t_f}{2} + t_f\right)\right), \quad \xi_s \in (-1,1). \tag{15}$$

4. Application of global time method

In order to resolve the solid and liquid domains, the Global Time Method, GTM, will be employed. This method has been applied to both direct and inverse problems [12,18–20], and has been found to produce stable and accurate results. The premise of the method is the classical weighted-residual method in which time is treated in an elliptic fashion. This treatment allows the resolution of the entire space–time domain simultaneously.

4.1. Liquid domain

To begin the formulation process, the unknown temperature field, $\theta_l(\eta_l,\xi_l)$, is assumed to be expressible as a series expansion of the form

$$\theta_l(\eta_l,\xi_l) = \sum_{k=0}^{\infty} a_k(\xi_l)T_k(\eta_l), \quad (\eta_l,\xi_l) \in [-1,1], \tag{16}$$

where Chebyshev polynomials of the first kind, $T_k(\eta_l)_{k=0}^{\infty}$, have been chosen as the global spatial basis functions. For computational purposes, an infinite

number of terms cannot be retained. Therefore, the series must be truncated after say $N+2$ terms. Denoting this approximation to $\theta_l(\eta_l, \xi_l)$ as $\theta_l^{N+1}(\eta_l, \xi_l)$, Eq. (16) can be rewritten as

$$\theta_l(\eta_l, \xi_l) \approx \theta_l^{N+1}(\eta_l, \xi_l) = \sum_{k=0}^{N+1} a_k^{N+1}(\xi_l) T_k(\eta_l), \quad (\eta_l, \xi_l) \in [-1, 1] \tag{17}$$

where $\lim_{N\to\infty} a_k^{N+1}(\xi_l) = a_k(\xi_l)$. To preclude the need for special treatment of the interfacial and initial conditions, e.g., boundary residual statements, the expansion can be modified to directly incorporate these conditions. This procedure also removes the introduction of errors into the solution from the boundaries. Forcing Eq. (17) to identically satisfy the interfacial conditions, Eqs. (6a) and (6b), performing some algebraic manipulations, and reindexing the series, we obtain

$$\theta_l^N(\eta_l, \xi_l) = \theta_{l_0}(\xi_l) + (\eta_l + 1)\Gamma_l(\xi_l) + \sum_{k=1}^{N} b_k^N(\xi_l)\omega_{l_k}(\eta_l), \quad (\eta_l, \xi_l) \in [-1, 1] \tag{18a}$$

where

$$\omega_{l_k}(\eta_l) = T_{k+1}(\eta_l) + (-1)^k\left(1 - (k+1)^2(\eta_l + 1)\right), \tag{18b}$$

$b_k^N(\xi_l) = a_{k+1}^{N+1}(\xi_l)$ and $\theta_l^N(\eta_l, \xi_l) = \theta_l^{N+1}(\eta_l, \xi_l)$. Next, we choose to express the time-varying expansion coefficients $\{b_k^N(\xi_l)\}_{k=1}^N$ as a series expansion of the form

$$b_k^N(\xi_l) = \sum_{j=0}^{P_k-1} c_{j,k}^N T_j(\xi_l), \quad \xi_l \in [-1, 1], \quad k = 1, 2, \ldots, N, \tag{19}$$

where Chebyshev polynomials of the first kind have been chosen as the global temporal basis functions. Substituting Eq. (19) into Eq. (18a) gives

$$\theta_l^N(\eta_l, \xi_l) = \theta_{l_0}(\xi_l) + (\eta_l + 1)\Gamma_l(\xi_l) + \sum_{k=1}^{N}\sum_{j=0}^{P_k-1} c_{j,k}^N T_j(\xi_l)\omega_{l_k}(\eta_l), \quad (\eta_l, \xi_l) \in [-1, 1]. \tag{20}$$

To incorporate the initial condition, a somewhat more complex series of operations is required as compared to incorporation of the interfacial conditions. The first step is to force Eq. (20) to identically satisfy the initial condition, Eq. (8),

$$\begin{aligned}\theta_l^N(\eta_{l_0}, -1) &= \theta_i(\eta_{l_0}) \\ &= \theta_{l_0}(-1) + (\eta_{l_0} + 1)\Gamma_l(-1) \\ &\quad + \sum_{k=1}^{N}\sum_{j=0}^{P_k-1} c_{j,k}^N T_j(-1)\omega_{l_k}(\eta_{l_0}),\end{aligned} \quad \eta_{l_0} \in [-1, 1]. \tag{21}$$

Subtracting Eq. (21) from Eq. (20) and noting that $T_j(-1) = (-1)^j$ gives

$$\begin{aligned}\theta_l^N(\eta_l, \xi_l) &= \theta_i(\eta_{l_0}) + \theta_{l_0}(\xi_l) - \theta_{l_0}(-1) \\ &\quad + (\eta_l + 1)\Gamma_l(\xi_l) - (\eta_{l_0} + 1)\Gamma_l(-1) \\ &\quad + \sum_{k=1}^{N}\sum_{j=0}^{P_k-1} c_{j,k}^N\left(T_j(\xi_l)\omega_{l_k}(\eta_l) \right. \\ &\quad \left. + (-1)^{j+1}\omega_{l_k}(\eta_{l_0})\right),\end{aligned} \quad (\eta_l, \xi_l) \in [-1, 1], \quad \eta_{l_0} \in [\Delta, 1], \tag{22}$$

where $\Delta = 2\frac{h_l(\xi_l)}{L} - 1$. Finally, reapplying the interfacial conditions to Eq. (22), solving for $\theta_{l_0}(-1)$ and $\Gamma_l(-1)$, and substituting the results back into Eq. (22) we obtain

$$\theta_l^N(\eta_l, \xi_l) = \psi_l(\eta_l, \xi_l) + \sum_{k=1}^{N}\sum_{j=1}^{P_k} d_{j,k}^N \Omega_{l_{j,k}}(\eta_l, \xi_l), \quad (\eta_l, \xi_l) \in [-1, 1], \tag{23a}$$

where

$$\psi_l(\eta_l, \xi_l) = \theta_i(\eta_{l_0}) - \theta_i(\Delta) + \theta_{l_0}(\xi_l) + (\eta_l + 1)\left(\Gamma_l(\xi_l) - \left(\frac{L - h_l(\xi_l)}{L}\right)\frac{\partial}{\partial \eta_{l_0}}\theta_i(\eta_{l_0})\bigg|_{\eta_{l_0}=\Delta}\right) \tag{23b}$$

and

$$\Omega_{l_{j,k}}(\eta_l, \xi_l) = T_{j-1}(\xi_l)\omega_{l_k}(\eta_l) + (-1)^j\left(\omega_{l_k}(\eta_{l_0}) - \omega_{l_k}(\Delta) - (\eta_l + 1)\left(\frac{L - h_l(\xi_l)}{L}\right)\frac{\partial}{\partial \eta_{l_0}}\omega_{l_k}(\eta_{l_0})\bigg|_{\eta_{l_0}=\Delta}\right). \tag{23c}$$

Since the expansion in Eq. (23a) identically satisfies all the interfacial and initial conditions, all that remains to fully resolve the liquid domain is the determination of the expansion coefficients. Towards this goal, orthogonal collocation will be called upon. For the application of orthogonal collocation, a residual statement must first be formulated. This is accomplished via the substitution of the assumed expansion, Eq. (23a), into the governing equation, Eq. (5a), and the addition of a residual function to maintain the equality. Performing these operations gives

$$R_{\mathrm{l}}^{N}\left(\theta_{\mathrm{l}}^{N}(\eta_{\mathrm{l}},\xi_{\mathrm{l}})\right)=\bar{\mathscr{L}}_{\mathrm{l}}\left[\theta_{\mathrm{l}}^{N}(\eta_{\mathrm{l}},\xi_{\mathrm{l}})\right],\quad (\eta_{\mathrm{l}},\xi_{\mathrm{l}})\in(-1,1). \tag{24}$$

In general, we cannot expect $R_{\mathrm{l}}^{N}(\theta_{\mathrm{l}}^{N}(\eta_{\mathrm{l}},\xi_{\mathrm{l}}))=0$ for $(\eta_{\mathrm{l}},\xi_{\mathrm{l}})\in(-1,1)$. Because of this, we seek to determine a set of expansion coefficients, which will minimize the residual function in some sense. For orthogonal collocation, we require that the residual function be orthogonal to a set of test functions with respect to the appropriate weight function. This can be written compactly using the inner product of two functions as

$$\langle R_{\mathrm{l}}^{N}\left(\theta_{\mathrm{l}}^{N}(\eta_{\mathrm{l}},\xi_{\mathrm{l}})\right),\delta(\eta_{\mathrm{l}}-\eta_{\mathrm{l}_m})\delta(\xi_{\mathrm{l}}-\xi_{\mathrm{l}_n})\rangle_{\mathrm{l}}=0,\quad m=1,2,\ldots,N,\quad n=1,2,\ldots,P_m, \tag{25}$$

where δ represents the Dirac delta function. The collocation points, $\{\eta_{\mathrm{l}_m}\}_{m=1}^{N}$ and $\{\xi_{\mathrm{l}_n}\}_{n=1}^{P_m}$, are defined according to the open rule as

$$\eta_{\mathrm{l}_m}=\cos\left(\frac{(2m-1)\pi}{2N}\right),\quad m=1,2,\ldots,N, \tag{26a}$$

$$\xi_{\mathrm{l}_n}=\cos\left(\frac{(2n-1)\pi}{2P_m}\right),\quad n=1,2,\ldots,P_m. \tag{26b}$$

Recognizing the 'sifting' nature of the Dirac delta function, substituting Eq. (23a) into Eq. (25) and using Eq. (24), the explicit matrix form for the resolution of the expansion coefficients becomes

$$\sum_{k=1}^{N}\sum_{j=1}^{P_k}d_{j,k}^{N}\bar{\mathscr{L}}_{\mathrm{l}}\left[\Omega_{\mathrm{l}_{j,k}}(\eta_{\mathrm{l}_m},\xi_{\mathrm{l}_n})\right]=-\bar{\mathscr{L}}_{\mathrm{l}}\left[\psi_{\mathrm{l}}(\eta_{\mathrm{l}_m},\xi_{\mathrm{l}_n})\right],\quad m=1,2,\ldots,N,\ n=1,2,\ldots,P_m. \tag{27}$$

Once the expansion coefficients have been determined via inversion of Eq. (27), the liquid domain can be reconstructed using Eq. (23a).

4.2. Solid domain

Owing to the similarity in the application of the GTM to the liquid domain, an in-depth exposition of the solid domain is not presented. Instead, a brief overview will be presented, which points out the significant differences between the two domains. As before, we begin by assuming a series expansion for the unknown temperature field in terms of a set of unknown time varying expansion coefficients and global spatial basis functions. Next, the series is truncated and algebraically manipulated such that it identically satisfies the boundary conditions in Eqs. (12a) and (12b). Thereafter, the time varying expansion coefficients are expanded into a series in terms of a set of unknown expansion coefficients and global temporal basis functions. We next wish to force the series to identically satisfy the initial condition in Eq. (13). It is the incorporation of this condition, where the solid and liquid differ. The solid domain allows incorporation using the same approach as that used for the boundary conditions, whereas, the liquid domain required a complex series of operations for incorporation of the initial condition. At this point, the series expansion for the unknown temperature identically satisfies all the necessary ancillary conditions and all that remains is the determination of the expansion coefficients. The formulation of the residual function, required by the weighted residuals technique, is accomplished through substitution of the series expansion into the governing equation, Eq. (11a), and the addition of the residual function to maintain the equality. The unknown expansion coefficients can then be obtained through the minimization of the residual function utilizing orthogonal collocation. Once obtained, the expansion coefficients can be used in the reconstruction of the unknown temperature field and calculation of the heat flux at the cold wall.

5. Results

To test the methodology presented above, two test cases were chosen to provide illustrative results. For both cases, the spatial extent was chosen as $L=38.1$ mm. The initial superheat distribution consisted of a linear profile with $T_{\mathrm{i}}(0)=T_{\mathrm{f}}$ and $G_{\mathrm{i}}=0.5$ K/mm. With these choices, it can be seen that $t_{\mathrm{f}}=t_{\mathrm{p}}$ and the interfacial temperature history becomes $T_0(t)=T_{\mathrm{f}}$. For the spatial extent and melt material chosen, the penetration time was over-estimated as $t_{\mathrm{p}}=14$ s. Design values for the interfacial velocity and liquid-side interfacial temperature gradient of $V_{\mathrm{d}}=0.2$ mm/s, and $G_{\mathrm{d}}=0.94$ K/mm, respectively, were utilized.

The two test cases are delineated by the temporal evolution of the interfacial velocity, $V(t)$, and the liquid-side interfacial temperature gradient, $G_{\mathrm{l}}(t)$. The

cases presented are similar to those investigated by the authors in [21] utilizing the Function Decomposition Method, FDM. The first test case utilizes values for t_v and t_g of 64 s and 82 s, respectively. The second test case, using values of $t_v = 37$ s and $t_g = 58$ s, explores the effects of shorter development times for the design velocity and the interfacial temperature gradient on the required hot and cold wall active control measures and the ability of the GTM to resolve these measures. To assure the majority of the domain would be solidified,

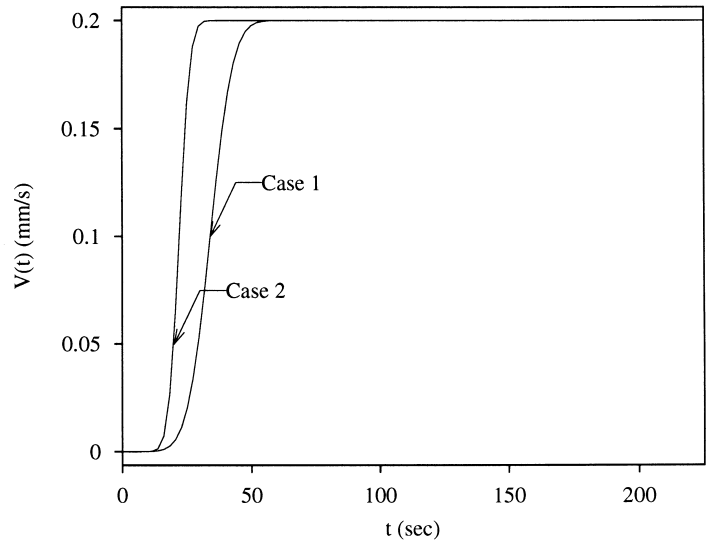

(a)

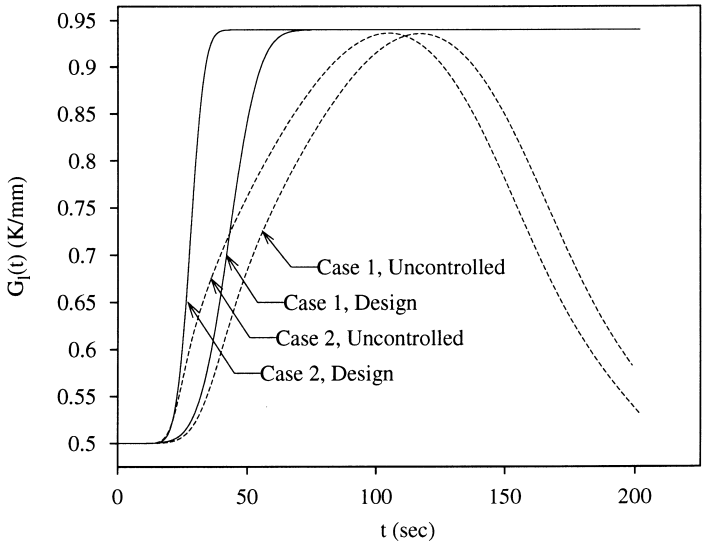

(b)

Fig. 3. Scenarios utilized in the investigation of the solidification design problem: (a) interfacial velocity; (b) liquid-side interfacial temperature gradient.

a maximum time of $t_{max} \approx 205$ s was chosen. The design velocity scenarios for both cases are shown in Fig. 3(a).

For the melt material, a lead–tin, PbSn, alloy of eutectic composition, 61.9 wt% Sn, was selected. For this material, the following physical properties, evaluated at its eutectic temperature of $T_f = 183°C$, were used [22]: $k_s = 28.530$ W/m K, $c_{p_s} = 165.72$ J/kg K, $k_l = 12.890$ W/m K, $c_{p_l} = 207.80$ J/kg K, and $h_f = 27837.35$ J/kg. Although the solid and liquid densities

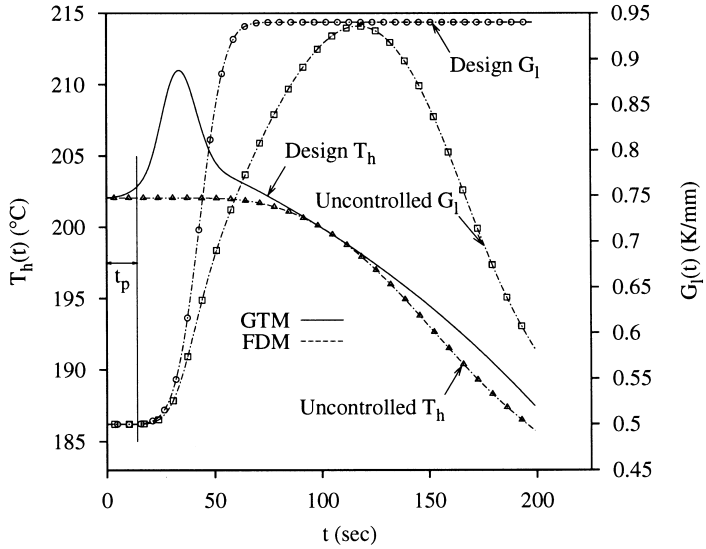

(a)

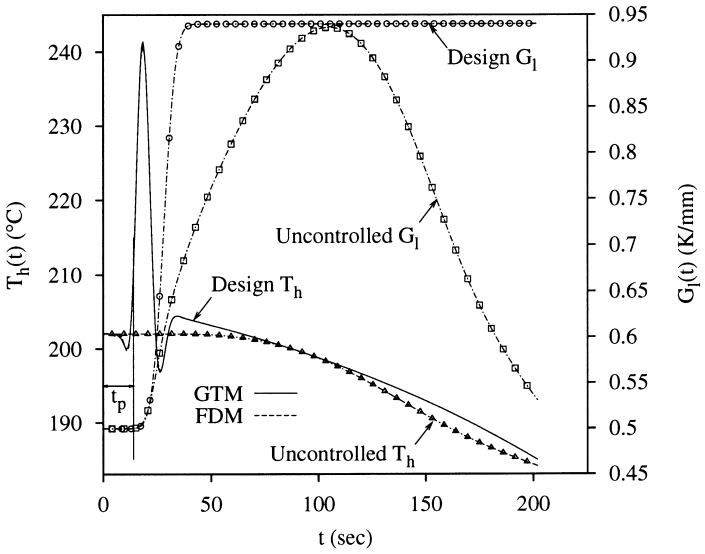

(b)

Fig. 4. Hot wall temperature history, $T_h(t)$, required to control solidification with respect to the liquid-side interfacial temperature gradient, $G_l(t)$: (a) case 1, $N = 10$, $P = 100$; (b) case 2, $N = 12$, $P = 150$.

are unequal, they are assumed equal to comply with the assumption of no bulk motion in the liquid region. Thus a constant value of $\rho = 8526.24$ kg/m^3 was utilized in the analysis.

A direct analysis of the liquid domain was conducted to provide a clear delineation between the design liquid-side interfacial temperature gradient and that which would occur if no active measures are taken on the hot wall, $x = L$. The direct analysis was based on the design interfacial velocity scenario, $V(t)$, interfacial temperature history of $T_0(t) = T_f$, initial linear temperature distribution with $T_i(0) = T_f$ and $G_i = 0.5$ K/mm, and a constant temperature gradient of 0.5 K/mm at the hot wall. Comparisons of the liquid-side interfacial temperature gradient, $G_l(t)$, under controlled, i.e., design scenario, and uncontrolled, i.e., direct analysis, conditions for both cases are presented in Fig. 3(b). The figure, clearly illustrates the differences in the desired temporal behavior of $G_l(t)$ and the behavior if no active control measures are taken at $x = L$. It also illustrates that case 2 requires an earlier initiation of the control, due to the earlier deviation of the design $G_l(t)$ from the uncontrolled behavior of the interfacial temperature gradient.

The active measures required to achieve a controlled solidification with respect to the liquid-side interfacial temperature gradient, $G_l(t)$, are shown in Fig. 4 and 5 along with those obtained by the authors utilizing the FDM [21]. Also, the results of the direct analysis discussed above are included in these figures for comparison. These figures reveal several important points which should be noted. Firstly, Fig. 4(a) and (b) clearly illustrate that the inclusion of the penetration time in the design scenarios is necessary. This is evidenced by the fact that active measures must be taken at the top wall, i.e., $T_h(t)$ deviates from the direct solution, almost immediately, $t \approx 0$ s, to effect a change in the liquid-side interfacial temperature gradient some time later in the transient, $t \approx 14$ s. If, on the other hand, the penetration time had not been included, i.e., the design liquid-side temperature gradient was chosen to deviate from the uncontrolled behavior at the start of the transient, no solution would be obtained. This is due to the fact that active measures required to effect this deviation would have occurred prior to the start of the analysis, i.e., at 'negative times'. Secondly, it can be seen that the establishment of the design liquid-side interfacial temperature gradient requires highly transient measures during the early parts of the transient, while its maintenance during the latter parts of the transient requires subdued control measures.

A comparison of the results obtained for cases 1 and 2 illustrate an important point from the standpoint of implementation. For case 1, Fig. 5 clearly shows that the heat flux is positive throughout the transient indicating that only heating is required at the top wall. However, for case 2 the figure clearly shows that the heat flux is negative for some portion of the transient indicating that both heating and cooling are required at the top wall. This is an important consideration

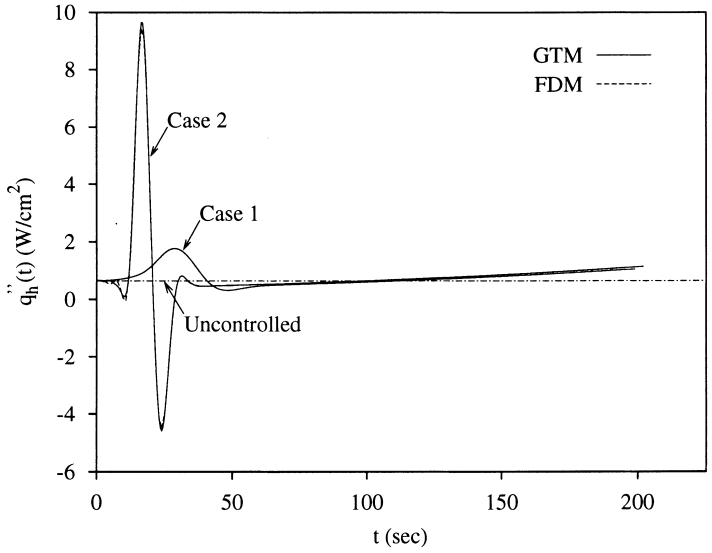

Fig. 5. Hot wall heat flux history, $q''_h(t)$, required to control solidification with respect to the liquid-side interfacial temperature gradient, $G_l(t)$. Note: $q''_h(t) > 0$ indicates heating.

when designing an apparatus to implement these control strategies. It is also noteworthy that even though the scenarios for cases 1 and 2 are similar in many aspects, the control strategies required to achieve the desired solidification, i.e., $T_h(t)$ and $q''_h(t)$, are markedly different and require varying levels of complexity with regards to the hardware implementation.

To achieve the desired interfacial motion, $s(t)$, during the solidification process, the active control measures shown in Fig. 6(a) and (b) must be applied.

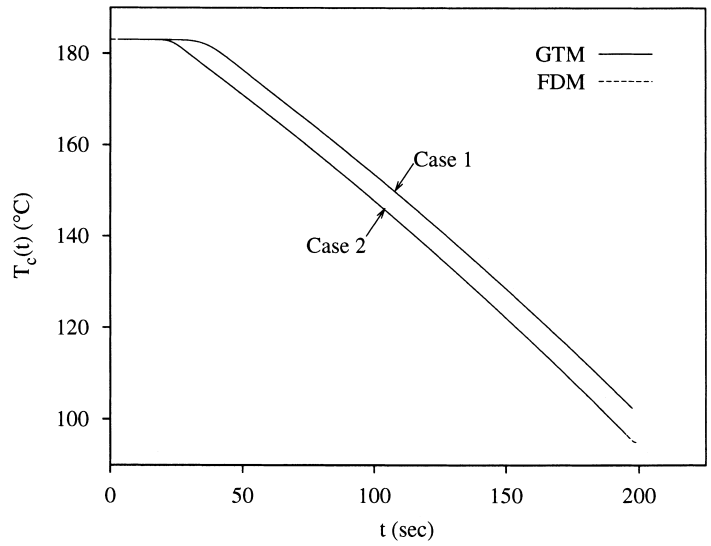

(a)

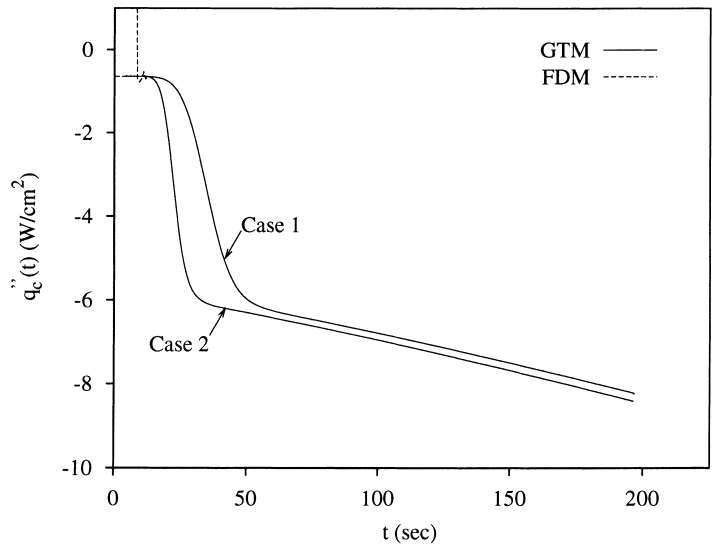

(b)

Fig. 6. Active measures required to control solidification with respect to the interfacial velocity, $V(t)$. Cases 1, 2: $N = 10$, $P = 100$: (a) cold wall temperature history, $T_c(t)$; (b) cold wall heat flux history, $q''_c(t)$. Note: $q''_c(t) < 0$ indicates cooling.

These results, illustrate that the differences in the liquid-side interfacial temperature gradient scenarios for cases 1 and 2, have minimal effect on the cold wall control strategy in that the overall character of the curves is maintained. This is expected, since the only difference between the two cases is the amount of time required for the design velocity to reach its constant design value of 0.2 mm/s. Recall that the value of t_v for case 2 is 27 s less than that for case 1.

To establish convergence of the results presented,

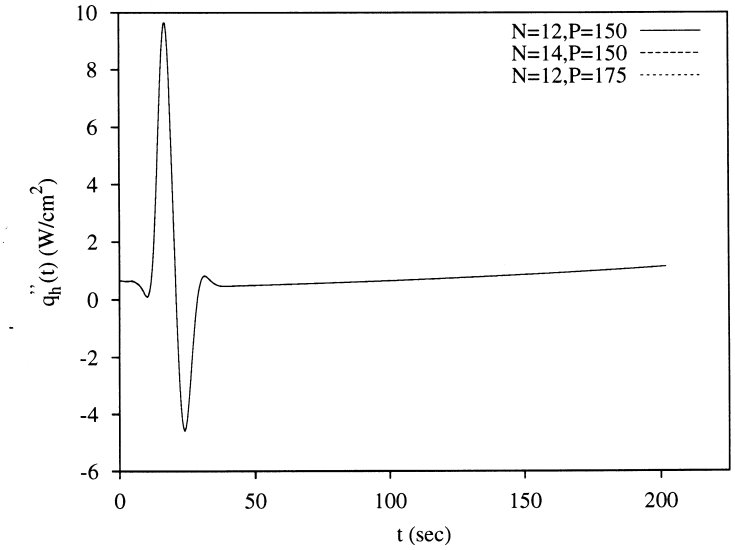

(a)

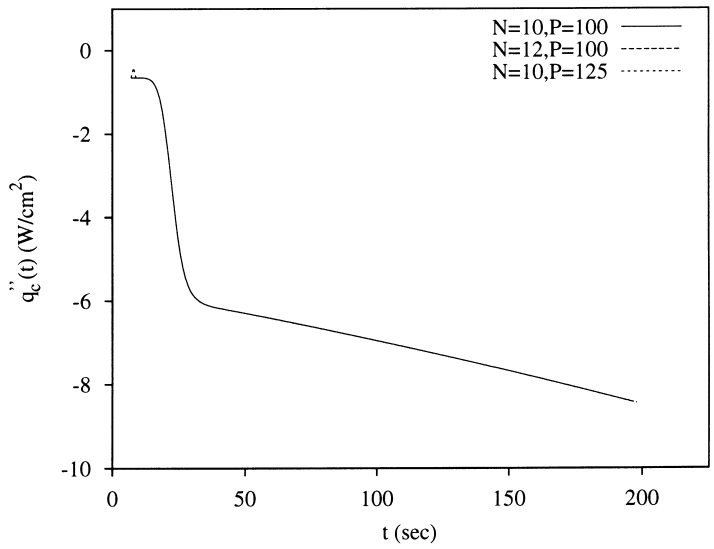

(b)

Fig. 7. Effect of N and P on the boundary heat flux prediction for case: (a) hot wall heat flux history, $q''_h(t)$; (b) cold wall heat flux history, $q''_c(t)$.

numerical experiments were performed. The results of these experiments for case 2 are shown in Fig. 7. For the hot wall active control, increasing N from 12 to 14 and P from 150 to 175 show no effect on the solution indicating convergence. Similarly, increasing N from 10 to 12 and P from 100 to 125 show no effect on the cold wall active control solution again indicating that convergence has been obtained. For case 1, similar results were obtained in that increasing the values of N and P above those presented provided no change in the solution.

In addition to illustrating convergence, the results of these additional runs indicate that the GTM is unaffected by the size of the 'time step', i.e., increasing P does not induce instability into the solution. This is a marked advantage of utilizing the GTM to solve this type of design problem over more traditional methods.

6. Conclusions

Though the test cases chosen are relatively simplified, they do illustrate the ability of the GTM to resolve this type of solidification design problem. Furthermore, the results obtained suggest that it is not only possible to independently control $V(t)$ and $G_1(t)$ during a casting process, but the active measures required to do so are not only physically realistic but relatively undemanding to implement in a laboratory setting. The authors plan future work, which will further illustrate the application of the GTM to more complex solidification design problems. Effects such as unequal phase densities, temperature dependent thermal properties, and the presence of a mushy zone, i.e., binary solidification, are currently under consideration. The inclusion of these effects will require the extension of the basic GTM to handle non-linear effects further illustrating its inherent flexibility.

Acknowledgements

The work presented in this paper was partially supported by the ALCOA Technical Center. The authors wish to thank Dr. Owen Richmond and Dr. Men G. Chu of the ALCOA Technical Center for their continued encouragement, support, and technical input.

References

[1] W. Kurz, D.J. Fisher, Fundamentals of Solidification, Trans. Tech. Publication, Switzerland, 1984.
[2] B. Chambers, Principles of Solidification, Wiley, New York, 1964.
[3] E.F. Bradley, High Performance Casting, ASM International, OH, USA, 1989.
[4] N. Zabaras, S. Mukherjee, O. Richmond, An analysis of inverse heat transfer problems with phase change using an integral method, Journal of Heat Transfer 110 (1988) 554–561.
[5] N. Zabaras, Y. Ruan, O. Richmond, Design of two-dimensional Stefan processes with desired freezing front motions, Numerical Heat Transfer, Part B 21 (1992) 307–325.
[6] N. Zabaras, Inverse finite element techniques for the analysis of solidification processes, International Journal for Numerical Methods in Engineering 29 (1990) 1569–1587.
[7] N. Zabaras, Y. Ruan, A deforming finite element method analysis of inverse Stefan problems, International Journal for Numerical Methods in Engineering 28 (1989) 295–313.
[8] N. Zabaras, S. Mukherjee, An analysis of solidification problems by the boundary element method, International Journal for Numerical Methods in Engineering 24 (1987) 1879–1900.
[9] N. Zabaras, S. Kang, On the solution of an ill-posed design solidification problem using minimization techniques in finite- and infinite-dimensional function spaces, International Journal for Numerical Methods in Engineering 36 (1993) 3973–3990.
[10] N. Zabaras, K. Yuan, Dynamic programming approach to the inverse Stefan design problem, Numerical Heat Transfer, Part B 26 (1994) 97–104.
[11] S. Kang, N. Zabaras, Control of the freezing interface motion in two-dimensional solidification processes using the adjoint method, International Journal for Numerical Methods in Engineering 38 (1995) 63–80.
[12] J.I. Frankel, M. Keyhani, A new approach for solving the inverse solidification design problem, Journal of Numerical Heat Transfer, Part B 30 (2) (1996) 161–177.
[13] J.V. Beck, B. Blackwell, C.R. St. Clair Jr, Inverse Heat Conduction, Ill Posed Problems, Wiley-Interscience, New York, 1985.
[14] H.S. Carslaw, J.C. Jaeger, Conduction of Heat in Solids, Clarendon Press, Oxford, 1959.
[15] V. Alexiades, A.D. Solomon, Mathematical Modeling of Melting and Freezing Processes, Hemisphere, Washington, 1993.
[16] G.Z. Yang, N. Zabaras, An adjoint method for the inverse design of solidification processes with natural convection, International Journal for Numerical Methods in Engineering 42 (1998) 1121–1144.
[17] G.Z. Yang, N. Zabaras, The adjoint method for an inverse design problem in the directional colidification of binary alloys, Journal of Computational Physics 140 (1998) 432–452.
[18] J.I. Frankel, G.E. Osborne, M. Keyhani, Thermal design aspects in inverse heat conduction, in: Third International Conference on Dynamic System Identification and Inverse Problems, Moscow, Russia, May 30–June 5, 1998.

[19] J.I. Frankel, M. Keyhani, A global time treatment for inverse heat conduction problems, Journal of Heat Transfer 119 (4) (1997) 673–683.
[20] J.I. Frankel, G.E. Osborne, A new time treatment for solving partial integro-differential equations of radiative transport, IMA Journal of Numerical Analysis 19 (1999) 91–103.
[21] S.W. Hale, M. Keyhani, J.I. Frankel, Application of the function decomposition method to design of solidification processes, in: Proceedings of the ASME Heat Transfer Division, HTD 361–5, 1998.
[22] M.C. Schneider, C. Beckerman, A numerical study of the combinded effects of microsegregation, mushy zone permeability and flow, caused by volume contraction and thermsolutal convection, on macrosegregation, and eutectic formation in binary alloy solidification, International Journal of Heat and Mass Transfer 38 (18) (1995) 3455–3473.